Inorganic Chemistry

Article

pubs.acs.org/IC

Kβ Valence to Core X-ray Emission Studies of Cu(I) Binding Proteins with Mixed Methionine − Histidine Coordination. Relevance to the Reactivity of the M- and H-sites of Peptidylglycine Monooxygenase

Vlad Martin-Diaconescu,[†,⊥,#] Kelly N. Chacón,[‡,⊥,▽] Mario Ulises Delgado-Jaime,[†,○] Dimosthenis Sokaras,[§] Tsu-Chien Weng,[§,◆] Serena DeBeer,*[,†,∥] and Ninian J. Blackburn*[,‡]

[†]Max Planck Institute for Chemical Energy Conversion, Stiftstraße 34-36, D-45470 Mülheim an der Ruhr, Germany

[‡]Institute of Environmental Health, Oregon Health & Sciences University, 3181 SW Sam Jackson Park Road, Portland, Oregon 97239, United States

[§]Stanford Synchrotron Radiation Lightsource, 2575 Sand Hill Road, Menlo Park, California 97025, United States

[∥]Department of Chemistry and Chemical Biology, Cornell University, Ithaca, New York 14853, United States

Supporting Information

ABSTRACT: Biological systems use copper as a redox center in many metalloproteins, where the role of the metal is to cycle between its +1 and +2 oxidation states. This chemistry requires the redox potential to be in a range that can stabilize both Cu(I) and Cu(II) states and often involves protein-derived ligand sets involving mixed histidine−methionine coordination that balance the preferences of both oxidation states. Transport proteins, on the other hand, utilize copper in the Cu(I) state and often contain sites comprised predominately of the cuprophilic residue methionine. The electronic factors that allow enzymes and transporters to balance their redox requirements are complex and are often elusive due to the dearth of spectroscopic probes of the Cu(I) state. Here we present the novel application of X-ray emission spectroscopy to copper proteins via a study of a series of mixed His-Met copper sites where the ligand set varies in a systematic way between the His_3 and Met_3 limits. The sites are derived from the wild-type peptidylglycine monooxygenase (PHM), two single-site variants which replicate each of its two copper sites (Cu_M-site and Cu_H-site), and the transporters CusF and CusB. Clear differences are observed in the $K\beta_{2,5}$ region at the Met_3 and His_3 limits. CusB (Met_3) has a distinct peak at 8978.4 eV with a broad shoulder at 8975.6 eV, whereas Cu_H (His_3) has two well-resolved features: a more intense feature at 8974.8 eV and a second at 8977.2 eV. The mixed coordination sphere CusF (Met_2His) and the PHM Cu_M variant (Met_1His_2) have very similar spectra consisting of two features at 8975.2 and 8977.8 eV. An analysis of DFT calculated spectra indicate that the intensity of the higher energy peak near 8978 eV is mediated by mixing of ligand-based orbitals into the Cu d^{10} manifold, with S from Met providing more intensity by facilitating increased Cu p−d mixing. Furthermore, reaction of WT PHM with CO (an oxygen analogue) produced the M site CO complex, which showed a unique XES spectrum that could be computationally reproduced by including interactions between Cu(I) and the CO ligand. The study suggests that the valence-to-core (VtC) region can not only serve as a probe of ligand speciation but also offer insight into the coordination geometry, in a fashion similar to XAS pre-edges, and may be sufficiently sensitive to the coordination of exogenous ligands to be useful in the study of reaction mechanisms.

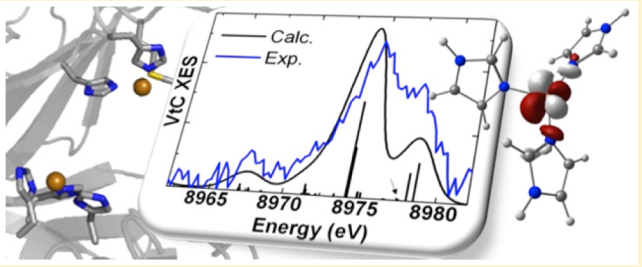

INTRODUCTION

Copper metal centers are present in a variety of metalloproteins, where they serve as redox centers, often cycling between the physiologically accessible +1 and +2 oxidation states. Oxidases bind molecular oxygen at Cu(I) sites and convert it to "activated" reduced forms, such as superoxo and peroxo species, which are reactive toward organic substrates. Electron transfer proteins utilize the two oxidation states to shuttle electrons from reductants into these catalytic sites. This chemistry requires a fine balance of coordinating ligands in order to set the redox potential at an appropriate level. Often a combination of histidine and methionine residues are utilized, which leverage the cupriphilic (Cu(II)) and cuprophilic (Cu(I)) properties of histidine and methionine, respectively. Separate systems have evolved to sequester and transport copper within the cell, and here the reduced Cu(I) state is preferred owing to the reducing environment of the cytoplasm. Predictably, these transport proteins favor Met ligation over His but often still exhibit mixed Met-His coordination at their Cu(I) binding sites. The detailed electronic factors that contribute to the stability and reactivity of Met/His ligand

Received: December 9, 2015
Published: March 11, 2016

DOI: 10.1021/acs.inorgchem.5b02842
Inorg. Chem. 2016, 55, 3431−3439

sets are important yet elusive factors underpinning the cellular chemistry of copper, due largely to a lack of experimental probes of the Cu(I) state. Here we use X-ray emission spectroscopy (XES) to study the ground-state properties of a series of Met/His copper binding sites derived from (a) the enzyme peptidylglycine monooxygenase and (b) the transporters CusF and CusB.

Peptidylglycine α-hydroxylating monooxygenase (PHM) catalyzes stereospecific α-C hydroxylation of C-terminal glycines, the first step in the α-amidation of neuropeptide hormones.[1,2] The molecular oxygen-dependent reaction requires 2 equiv of ascorbate as an exogenous reductant, releasing water and semidehydroascorbate as byproducts. Crystallographic characterization reveals two distinct Cu centers in the protein active site separated by 11 Å.[3,4] The Cu_H site, believed to serve primarily as an electron transfer site, is coordinated by three histidines (His; H107, H108, H172) in a roughly "T-shaped" geometry. The Cu_M site, where oxygen binding and hydroxylation occur,[5] has a mixed coordination sphere consisting of two histidines (H242, H244) and a methionine (Met; M314) (Figure 1). Spectroscopic studies on the cupric and cuprous forms of the enzyme have provided oxidation-state-specific structural information.[6−10] In the oxidized form the Cu_M center is bound by two His residues and two water molecules in what appears to be a tetragonal geometry with a long axial bond to the Met residue, while on reduction the water ligands dissociate and the thioether of M314 moves closer to the copper. For the Cu_H site, the oxidized structure coordinates a water ligand in addition to its three His residues to complete the 4-coordination expected for a Cu(II) center, and on reduction this water is again lost. Exogenous ligands (O_2, CO, peroxide, azide) bind to the catalytic Cu_M site but appear to be excluded from the electron transfer Cu_H site by electronic or steric factors which are not well understood.[5,10−13]

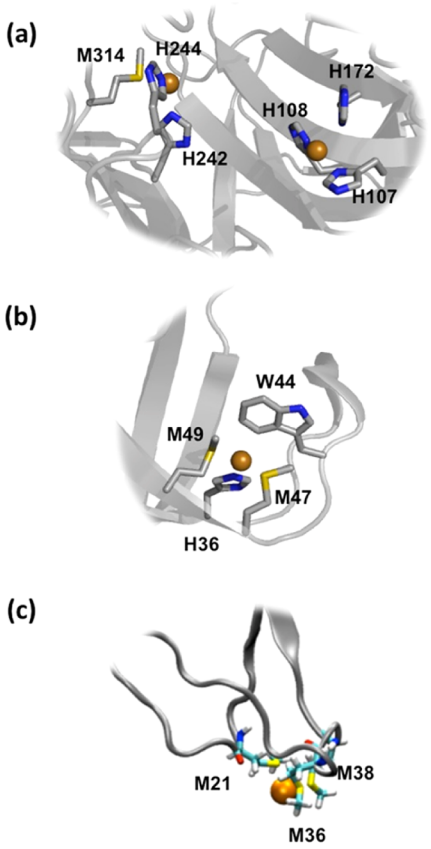

Figure 1. (a) WT PHM metal binding sites (PDB: 1PHM). (b) CusF metal binding site (PDB: 2VB2). Color scheme: sulfur, yellow; nitrogen, blue; copper, orange. (c) In silico CusB metal binding site (adapted from ref 23; reprinted with permission, copyright 2013 American Chemical Society).

The *cus* operon of *E. coli* encodes four structural genes—*CBAF*—where CusCBA forms a tripartite complex that spans the periplasmic space and imparts resistance to both Ag(I) and Cu(I).[14−16] The metallo sites of the components of the Cus system have a rich coordination chemistry, which is dominated by methionine ligation. CusF, which serves as a periplasmic metallochaperone, coordinates a single Cu(I) or Ag(I) ion in a $(Met)_2His$ environment but the site is capped by a unique π-cation interaction with a tryptophan residue (Figure 1b).[17−19] CusB, a periplasmic membrane fusion protein, contains three conserved Met residues (M21, M36, M38) in its disordered N-terminal domain, which have been implicated as the binding site for Cu(I) and Ag(I) by XAS (Figure 1c).[20−22] DFT and QM/MM calculations have provided further insight through in silico structures of the CusB N terminus in both apo- and metal-bound forms,[23] where metal binding appears to induce a significant structural rearrangement suggestive of a function involving a metal-induced conformational switch. The CusA metal binding site, as determined from crystal soaks, lies within a deep cleft in the periplasmic domain and is suggested to consist of three Met residues, although other potential ligands (particularly E625) are within coordinating distance.[24,25] Completing the tripartite complex, an outer membrane channel is proposed to be formed by a trimeric assembly of CusC.[26] Recent multiedge XAS studies have firmly established the individual roles of the protein components of the transporter.[27] CusF is able to sense the periplasmic metal load and under high flux transfers Cu(I)/Ag(I) to CusB, generating an active CusB conformer which binds to CusA and activates the pump. The activated form of CusA can now also accept metal from the CusF chaperone and transport it out of the cell. However, as the periplasmic metal flux falls, back-transfer from B to F leads to the apo form of CusB, which can no longer interact with CusA and shuts off further transport. For the current study, the Met_2His and Met_3 ligand sets of CusF and CusB, respectively, are uniquely suitable for studying the electronic interactions of the d^{10} Cu(I) in mixed thioether and imidazole ligand environments.

To understand the role of His and Met residues in copper-based catalytic and transport systems in more detail, Kβ valence-to-core (VtC) XES was applied as a direct probe of ligand coordination environment and electronic structure. Kβ VtC XES is due to transitions from valence electrons to the metal 1s core-hole.[28,29] This method has previously been used to identify the presence of a bridging oxygen atom in the OEC, the protonation state of oxo-bridged Mn(IV) dimers, and the presence of a central carbon in nitrogenase.[30−33] Data were collected and analyzed for WT PHM, and two recently characterized variants in which only the Cu_M site (H107AH108A) or only the Cu_H site (H242A) was occupied, providing His_2Met and His_3 isolated ligand sets,[9] and on wild type PHM with CO bound to the Cu_M site (PHM-CO)[12] as a model for the PHM-dioxygen catalytic complex. These systems were compared with CusF (Met_2His) and CusB (Met_3), providing a systematic series of Cu(I) coordination spheres

DOI: 10.1021/acs.inorgchem.5b02842
Inorg. Chem. 2016, 55, 3431−3439

ranging from His_3 to Met_3 to facilitate spectral analysis. Correlation of the experimental spectra with theoretical calculations allowed a comparison of the Cu−ligand binding interaction for methionine versus histidine, determined contributions to the spectra from metal d orbitals, and showed how these contributions are affected by ligand orientation and binding mode. Finally, the sensitivity of VtC XES to detect small-molecule binding in PHM was investigated, as a prelude to future mechanistic studies. To the best of our knowledge, this represents the first VtC XES application to copper proteins; however, previous studies have shown the potential of Cu VtC XES by exploring the ligand protonation state in Cu(II) models of galactose oxidase.[34]

EXPERIMENTAL SECTION

Protein Expression and Sample Preparation. *Preparation of PHM Samples.* WT PHM and its single-site variants were prepared as described previously.[9] Protein expression was carried out in hollow fiber bioreactors[6,35,36] as follows. The stably transfected cell lines were thawed from freezer stock into a T75 flask with 20 mL of DMEM/F12 medium containing 10% FCII serum (Fisher). At 80% confluence, the cells were passed into five NUNC triple flasks (500 cm^2 per flask), which were also grown to confluence. The cells were trypsinized and resuspended in 50 mL of DMEM/F12 medium with 10% FCII serum prior to inoculation into the extra-capillary space (ECS) of a Hollow Fiber Bioreactor (Fibercell Systems 4300-C2008, MWCO 5kD, 3000 cm^2 surface area) precultured with 2 L of 50 mM PBS pH 7.35 and 2 L of DMEM/F12 10% FCII serum.[7,12,35] Individual bioreactors containing each of the variants were fed with DMEM/F12/10% FCII serum for 1 month. The serum level was then reduced to 0.5%, at which point spent medium (20 mL) from the ECS was collected every other day and frozen at −20 °C for later purification. About 1 month's worth of the bioreactor harvest (300 mL) for each variant was purified as previously described.[7,12,35] Copper reconstitution was carried out as follows. For WT PHM, purified enzyme was dialyzed against 20 mM sodium phosphate buffer (pH 8.0) and then reconstituted with 2.5 mol equiv of Cu(II) sulfate per protein followed by two cycles of dialysis to remove unbound cupric ions. For the single-site variants (H107AH108A and H242A), the purified protein was initially dialyzed against 20 mM sodium phosphate buffer (pH 8.0) overnight and reconstituted with 2.5 equiv of Cu(II) sulfate using a syringe pump, at a rate of 60 μL/h, followed by exhaustive dialysis against copper-free phosphate buffer at the same pH and ionic strength. This procedure resulted in copper to protein ratios close to 1. Thereafter, the single-site mutants were reconstituted with 1.3 equiv of Cu(II) sulfate and dialyzed overnight against 20 mM sodium phosphate buffer (pH 8). The copper concentrations were determined using a PerkinElmer Optima 2000 DV inductively coupled plasma optical emission spectrometer (ICP-OES). Protein concentration was determined on a Cary-50 UV−vis spectrophotometer at room temperature using an extinction coefficient for a 1% solution at 280 nm of 0.980.

Reduced (Cu(I)-containing) derivatives were generated by reduction with a 5-fold excess of ascorbate buffered at the same pH as the protein sample. The protocol was carried out under anaerobic conditions to avoid air oxidation. The carbon monoxide derivative of the reduced enzyme was prepared by first vacuum-flushing the sample with argon and then incubating under 1 atm of CO gas for 15 min. All samples were flash-frozen in 2 mm × 10 mm lucite cuvettes immediately after preparation.

Preparation of CusF and CusB. The study utilized a variant of CusF missing its first five amino acid residues ($CusF_{6-88}$, hereafter termed CusF) and an N-terminal truncation variant of CusB (CusB-NT_{1-61}, hereafter termed CusB). *E. coli* BL21 (λDE3) cells containing the *$CusF_{6-88}$-trx-his6-tev* plasmid were grown from a freshly streaked plate into LB media containing 100 μg/mL of ampicillin at 37 °C until they reached an OD_{600} of 0.8, at which point protein expression was induced with 0.4 mM of isopropyl β-D-1-thiogalactopyranoside (IPTG). Growth was continued at 37 °C for 4 h, after which the cells were harvested by centrifugation and pelleted. The cells were resuspended, lysed using the French pressure method, and centrifuged to remove cell debris. The filtered supernatant was poured over a Ni-NTA resin column, rinsed with buffer, and eluted using a 250 mM imidazole buffer rinse. To remove the His6-Trx tag, tobacco etch virus (TeV) protease and 5 mM β-mercaptoethanol were added to the protein solution and the mixture was incubated at 20 °C overnight. After dialysis the protein solution was repurified on a Ni-NTA resin column, which removed the cleaved His tag to yield pure apo CusF. The CusB-NT protein was purified from the CusB-NT-*trx-his6-tev* plasmid in the same manner as for CusF.

Cu(I) forms of CusF and CusB-NT were prepared as follows. The protein concentration was determined by the BCA method, and then aliquots of appropriate concentration and volume were kept chilled overnight in a Coy anaerobic chamber to give anaerobic protein. Tetrakis(acetonitrile)copper(I) hexafluorophosphate (Cu(I)-ACN) was dissolved in pure acetonitrile and the amount of Cu(I)-ACN to add to the protein calculated such that the final ACN concentration was 10% of the total protein solution by volume. The Cu(I)-ACN was added to the apo protein anaerobically by syringe pump (1 μL/min rate), with stirring, at a ratio of 1.5:1 metal to protein. The mixture was then incubated an additional 1 h with stirring, over ice. The metalated proteins were concentrated to the desired volume using a micro-concentrator, and three cycles of desalting were accomplished using spin columns using buffer containing 10%, 5%, and 0% acetonitrile, respectively, which removed excess metal and salt from the proteins. The proteins were then flash-frozen in XES sample cuvettes. Metal to protein concentrations were verified by ICP-OES and the BCA or Bradford assay.

X-ray Emission Data Collection. The XES experiments were performed on beamline 6-2 at the Stanford Synchrotron Radiation Lightsource with an operating ring current of 500 mA. The beamline delivered to the sample spot an incident X-ray beam of 10.5 keV with ~10^{13} photons/s via a liquid N_2 cooled Si(111) monochromator, focused to ~250 × 700 μm^2 (fwhm) by means of a Rh-coated Si mirror. The Si(111) monochromator was calibrated using the X-ray absorption of a metallic Cu foil with the first infection point set to 8978.9 eV. Then the monochromator energy was scanned through the energy range of the Kβ emission, and the XES spectrometer was calibrated using elastic scattering peaks at each monochromator position. The samples were kept at a temperature of 10 K using a liquid He flow cryostat. Multiple spots on each sample were used for collecting an overall (averaged) XES spectra as follows. First, a spot in the center of the sample was chosen and scanned between 8875 and 8930 eV in 0.25 eV steps counted for 1 s per step, to collect a spectrum of the Kβ mainline. Data collection was then switched to the VtC region, which was scanned between 8925 and 9020 eV in 1.5 eV steps, counted for 2 s per step. The 5 eV overlap between mainline and VtC regions ensured that VtC spectra could be normalized to the intensity of the mainline peak. For VtC spectra, a total of 32 independent spots were measured per sample, with two scans collected per spot for a total of 64 scans per sample. These were subsequently averaged to generate an overall VtC spectrum for each sample. The total dose per exposed spot was below the radiation damage threshold, as determined with consecutive XES spectra and/or XAS time scans monitored using the shape of the absorption edge feature at 8983 eV in a separate absorption scan. This procedure indicated that the fully reduced (Cu(I)) proteins were resistant to radiation damage over the time course of the XES data collection.

The XES spectra were recorded using a BL 6-2 multicrystal Johann spectrometer[37] employing six Si(551) spherical analyzers (100 mm in diameter with a 1 m radius of curvature) aligned on intersecting Rowland circles. A silicon drift detector was used at the focus of the spectrometer for recording the analyzed photons. A He-filled polyethylene bag was placed between the cryostat and the spectrometer to minimize signal attenuation and diffused scattering contribution from air. The energy resolution of the spectrometer was determined to be ~1 eV (fwhm) via elastic scattering scans along the energy range used for the Cu VtC XES.

DOI: 10.1021/acs.inorgchem.5b02842
Inorg. Chem. 2016, 55, 3431−3439

Data Processing. The Cu Kβ XES data were fit using a holistic model that included pseudo-Voigt functions to account for all the Kβ XES features and an offset, which accounted for Kα XES intensity. The differences in effective concentration (due to measurements on different sample spots) were accounted for by the use of a floating parameter in the fit model, which allowed for the alignment of VtC and Kβ mainline scan regions. To better highlight the intensity distributions of the VtC features, the Kβ mainline was subtracted and the total area under the VtC region between 8960 and 8985 eV was parametrized to reflect 1 unit of normalized intensity. Two spectral features (above 8980 eV) attributed to K+L excitations were included in the model, but the parametrization of their intensities was not included in the total (Kβ+VtC) intensity. Using Blueprint XAS, the solution space and the uncertainty of the fit parameters were explored by obtaining a large family of good fits based on the sum of squared errors, as previously described.[38,39] The fitted offset, mainline spectral contributions were then subtracted to better highlight the VtC region for each spectrum. The averages for the good fits for all spectra are provided in section S1 of the Supporting Information).

Theoretical Calculations. All theoretical calculations were carried out with the ORCA 3.0 computational chemistry package.[40] Geometry optimizations were carried out for each metal site using the first coordination sphere amino acid residues from crystal structures where available and a Cu(I) metal center. For CusB, the starting geometry for the metal binding site was approximated as trigonal planar using previously reported experimental bond distances and theoretically determined geometry coordination.[20,23] The BP86 functional[41,42] was used for all calculations. For geometry optimizations the backbone α carbons were frozen and the def2-TZVP basis set[43,44] was used for the metal center and directly coordinating atoms, while the def2-SVP set was employed for the remaining atoms. Solvation effects were accounted for using a conductor-like screening model (COSMO) with a dielectric constant of 30, approximating what is expected at the protein surface.[45] The geometry-optimized structures were then used to calculate the VtC XES spectra using the def2-TZVP basis set on all atoms. The VtC XES spectra were calculated within the single-point calculation routine using a one-electron theoretical protocol.[46] In order to facilitate facile comparison with experimental spectra, individual transitions for calculated spectra were described using a Gaussian peak function having a 2.6 eV fwhm, and the sum total of the transition intensities in the VtC region was normalized to 1. The overall experimental resolution, accounting for both spectrometer broadening (1 eV) and the Cu 1s core-hole lifetime (1.55 eV), is expected to be 1.85 eV. Therefore, the broadening applied to the calculated transitions suggests that the spectral features are not limited by the experimental resolution. Furthermore, correlation of calculated transitions to orbitals and model studies to investigate the effect of binding mode were carried out on truncated models of the metal sites with imidazoles and methyl thioethers replacing histidines and methionines, respectively. No significant deviation in calculated VtC XES spectra was observed to be due to the truncation (section S6 of the Supporting Information).

RESULTS AND DISCUSSION

Previous XAS Studies. Before discussing the present XES data, it is useful to briefly summarize previous Cu K-edge XAS studies on CusB (Met_3), CusF (Met_2His), and the PHM variants Cu_M (Met_1His_2) and Cu_H (His_3) bound to Cu(I).[9,17,20] In all cases, the XAS spectra are consistent with a three-coordinate Cu(I) center. This is supported by both a lack of any pre-edge features attributable to 1s → 3d transitions and a well-resolved feature at ~8983 eV attributed to a 1s → 4p transition.[47] Furthermore, in the case of the PHM Cu_M site, binding of CO leads to a decrease in the intensity of the ~8983 eV feature consistent with an increased coordination number dominated by a nitrogen, oxygen, or carbon ligand sphere.[47] We emphasize, however, that while XAS is a powerful probe of coordination environment and bond metrics, the lack of a pre-edge in the d^{10} system limits the quantitative information that can be obtained on the local site symmetry. Hence, the present study was initiated in order to determine the complementary information that can be obtained by using Cu Kβ XES to directly probe the filled orbital in a closed-shell d^{10} system.

Kβ XES Spectra. Kβ XES spectra have two parts, the mainline (or $Kβ_{1,3}$ region) consisting of emission lines from the filled metal 3p orbitals and the valence to core (VtC or $Kβ_{2,5}$+Kβ″) region corresponding to transitions from filled valence orbitals.[48,49] Mainlines can provide insight into the spin state and covalency at the metal center governed by a p−d exchange coupling.[49] However, in the present case the d^{10} configuration at the Cu(I) results in $Kβ_{1,3}$ mainlines which are superimposable and do not show any observable spectral changes due to changes in the ligand coordination environment (Figure 2). The $Kβ_{1,3}$ mainlines for all proteins in the present series have an intense peak at 8905.9 eV, a shoulder at ~8903.6 eV, and an additional weak shoulder at 8897.9 eV.

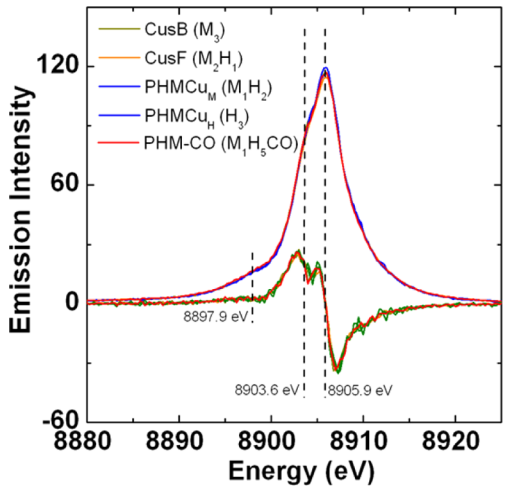

Figure 2. Experimental mainline $Kβ_{1,3}$ XES spectra and first derivatives highlighting features of interest. (M_1H_5CO) refers to the presence of both the Cu_M (M_1H_2) and Cu_H (H_3) sites with a CO molecule bound to Cu_M. Spectra were normalized by setting the total area under the curve (VtC + mainlines) to 1000.

VtC XES Spectra. Figure 3 shows the VtC spectra for CusB (Met_3), CusF (Met_2His), and the PHM variants Cu_M (Met_1His_2) and Cu_H (His_3). All spectra exhibit features in the $Kβ_{2,5}$ region (~8965−8980 eV), which are usually associated with transitions from ligand *n*p orbitals to the 1s core-hole of the metal. The energy positions for VtC features are generally correlated with the ligand ionization potential, while the intensity is highly dependent on metal−ligand bond distance.[46,50] Hence, the systematic variation in ligand speciation for the present series should provide insights into the nature of histidine versus methionine metal coordination. In particular, clear differences are observed in the VtC region at the Met_3 and His_3 limits. CusB (Met_3) has a distinct peak at 8978.4 eV with a broad shoulder at 8975.6 eV. Cu_H (His_3) has two well-resolved features: a more intense feature at 8974.8 eV and a second at 8977.2 eV. The mixed coordination sphere CusF (Met_2His) and the PHM Cu_M variant (Met_1His_2) have very similar spectra consisting of two features at 8975.2 and 8977.8 eV. The picture becomes more complex in mixed coordination spheres, as both the nature of the ligand and variations in metal−ligand distance are known to influence the

DOI: 10.1021/acs.inorgchem.5b02842
Inorg. Chem. 2016, 55, 3431−3439

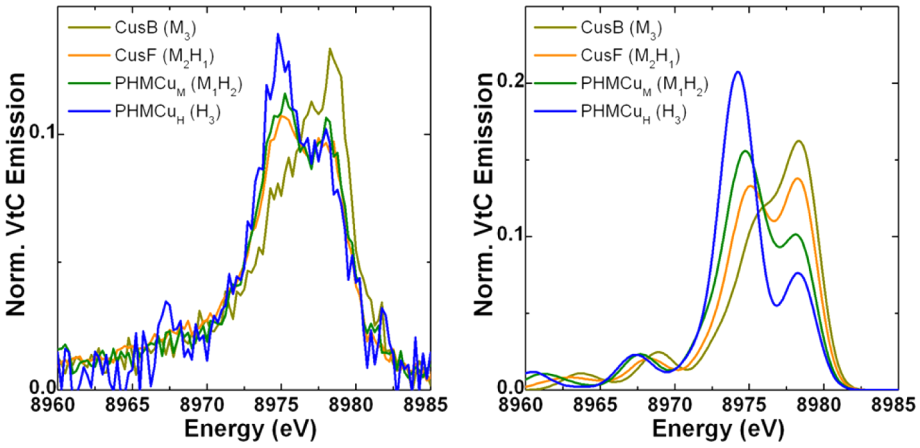

Figure 3. (left) Experimental VtC XES spectra. (right) Calculated VtC XES spectra. Calculated spectra are shifted by 232 eV.

spectra.[31,39,46,51] Figure 3 (right) also shows the calculated VtC XES spectra, for the series of Cu proteins. The trends from the calculations generally agree well with experiment, with the exception of CusF (Met_2His), where the intensity of the high-energy VtC feature seems to be overestimated. To help understand the contributions from the methionine and histidines to the VtC spectra, the principal calculated transitions to the CusB and Cu_H spectra were analyzed further.

Theoretical Assignment of VtC XES Spectra. In order to simplify the orbital picture, hisitidnes were approximated as imidazoles and methionines as methyl thioethers. No significant deviation in calculated VtC XES spectra was observed to be due to the truncation. Figure 4 shows an overlay of the calculated and experimental spectra for the trigonal-planar CusB Met_3 site. A breakdown of the transitions that contribute to the VtC region reveals four primary sets of transitions, as shown in Figure 4 (bottom). As the calculation uses a one-electron approximation, the transitions can be correlated with molecular orbitals.[39,46] The two most intense features, which appear at ~8978.4 eV and at ~8975.6 eV, correspond to transitions from the antibonding (**1**) and bonding (**3** and **4**) combinations of the $d_{x^2-y^2}$ and d_{xy} orbitals with the S 3p of the methionines, respectively. Two distinct sets of S 3p orbitals are involved, a lone pair S 3p orbital (**3**) and a S 3p orbital from the S−CH_3 σ bond (**4**). Transitions from these orbitals gain intensity due to the relatively high percentage of Cu p character present in these molecular orbitals. In D_{3h} symmetry the $d_{x^2-y^2}$ and d_{xy} orbitals have the appropriate symmetry to mix with metal p orbitals, and in a configuration interaction based model, these transitions can gain intensity through covalent ligand interactions, which serve as an intermediary to promote p−d mixing in appropriate symmetry.[52] In this context, one notes that both the Cu p and S p characters in these orbitals are significant (Figure 4 (middle)). In contrast, transitions from the antibonding and bonding combination with the d_{xz}, d_{yz}, and d_{z^2} set (**2**), which are not of appropriate symmetry to interact with the metal p orbitals, do not have significant intensity.

Similarly for Cu_H, which has a coordination sphere consisting of three histidines (imidazoles), the calculated spectrum accurately predicts the two experimentally observed features (Figure 5). Again the two most intense transitions (**1′** and **4′**) correspond to transitions from the antibonding and bonding combinations, respectively, of the $d_{x^2-y^2}$ and d_{xy} orbitals with the ligand. We note, however, that the imidazole character in the $d_{x^2-y^2}$ and d_{xy} orbitals is much less (~14%) than for the

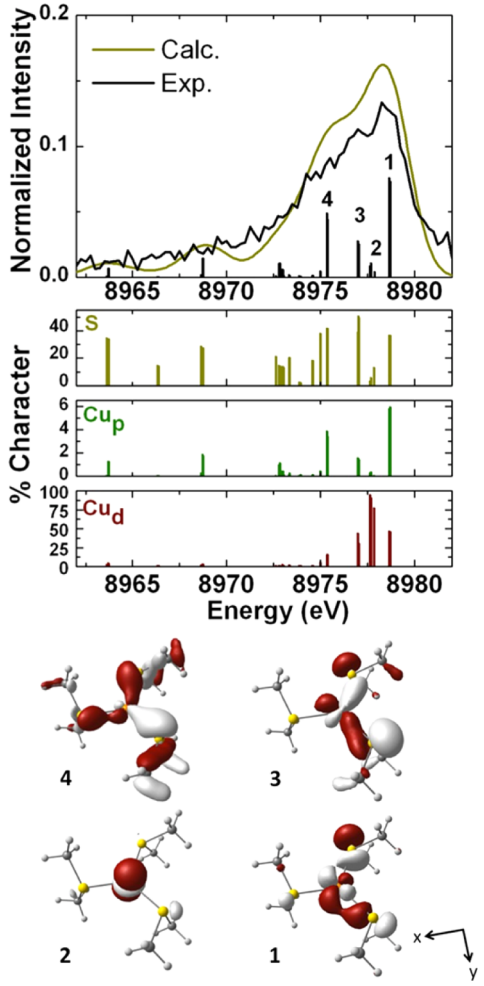

Figure 4. (top) Overlay of the experimental and calculated K$\beta_{2,5}$ VtC XES for CusB. The calculated spectra are shifted by 232 eV, and individual transitions are shown as sticks. The truncated model was used. (middle) Percent character breakdown for individual transitions. (bottom) Selected molecular orbitals corresponding to transitions of interest (isovalue 0.05).

methionine (thioether) ligands (~35%), resulting in less p−d mixing and lower overall transition intensities. In contrast to methionine, the most intense set of transitions in the Cu_H VtC spectra (**4′**) come from the N−$(CH_2)_2$ σ-bonding orbitals.

DOI: 10.1021/acs.inorgchem.5b02842
Inorg. Chem. 2016, 55, 3431−3439

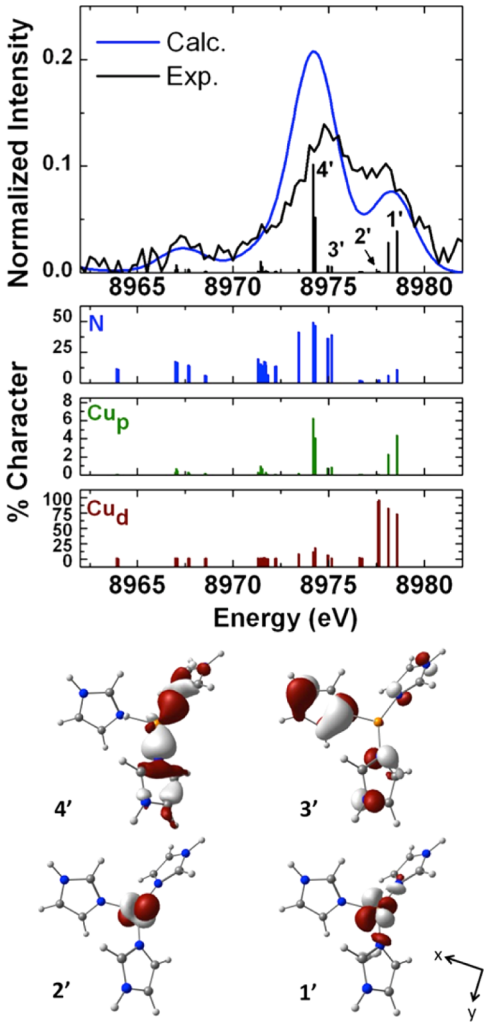

Figure 5. (top) Overlay of the experimental and calculated K$\beta_{2,5}$ VtC XES for Cu_H. The calculated spectra are shifted by 232 eV, and individual transitions are shown as sticks. The truncated model was used. (middle) Percent character breakdown for individual transitions. (bottom) Selected molecular orbitals corresponding to transitions of interest (isovalue 0.05).

These form a σ-bonding interaction with the Cu (and a corresponding antibonding interaction in **1**′). The equivalent of the S p lone pair for the metal-bonded N in imidazole (**3**′) does not interact strongly with the metal, as it forms part of the aromatic π manifold of the imidazole ring (Figure 5, bottom). Furthermore, the weak metal−ligand interaction that is present is a π-type interaction, which does not favor mixing with Cu p orbitals, and as previously described results in further loss of VtC intensity.[39,48]

Effect of Ligand Geometry on the Line Shape of Cu(I) VtC XES Spectra. Generally, for VtC XES the transition intensities and energies have been correlated with two principal factors: the metal−ligand bond distance and the ligand ionization potential.[28,46,50] For the former, the shorter the bond distance, the more metal character *n*p can mix into the orbital, resulting in a more intense transition. For the latter, the higher the ionization potential of the ligand, the lower in energy the corresponding VtC features appear. However, in the current study, the higher energy VtC features arise from filled metal d orbitals, which have ligand-mediated p mixing. Although the metal d manifold is not generally expected to contribute significantly to the VtC spectra, VtC features from metal d orbitals have previously been reported in iron−carbonyl complexes and more recently in a series of manganese dioxygen activating small molecules.[39,53] This effect is expected to become more pronounced, as in the current case, when a filled d^{10} shell is present. Therefore, a third factor also affects the Cu(I) VtC line shape: ligand-mediated metal p−d mixing.

To further investigate this factor, and in turn to help potentially explain some of the discrepancies in the calculated and experimental spectra, variations in the ligand geometry and their effect on the VtC XES were explored using model systems. A simplified model of the CusF metal binding site consisting of an imidazole and two thioethers was built and the geometry was allowed to relax, resulting in a S−Cu−S angle of 116°. Variation of the S−Cu−S angle was found to result in markedly different "Cu d" VtC features (Figure 6). This can be

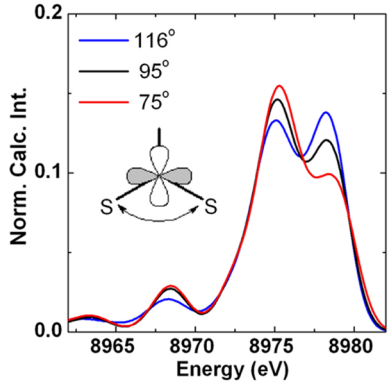

Model	$d_{x^2-y^2}$		d_{xy}	
	%d	%p	%d	%p
116°	58.5	4.6	52.5	6.0
95°	65.1	3.2	48.7	6.7
75°	68.6	1.7	43.4	6.8

Figure 6. (top) In silico study of the effect on the CusF VtC XES spectra of S−Cu−S angle variations and relative orientation of the $d_{x^2-y^2}$ orbital with respect to the S ligands (inset). (bottom) Percent Cu d and p character mixed in the d_{xy} and $d_{x^2-y^2}$ orbitals. Calculated spectra are shifted by 232 eV.

rationalized in terms of ligand-mediated Cu p−d mixing, dependent on the overlap between the S p-type orbitals with the Cu d manifold. In the case of a S−Cu−S angle of 116°, the $d_{x^2-y^2}$ orbital interacts predominantly with the histidine; however, some methionine character is also present. The methionine ligands, on the other hand, interact more directly with the d_{xy} orbital. A contraction of the S−Cu−S angle is predicted to reduce the amount of methionine sulfur mixing into the $d_{x^2-y^2}$ orbital, which in turn significantly lowers the amount of Cu p mixing (Figure 6 (bottom)). The d_{xy} orbital, pointing at the methionine ligands on the other hand, is largely unaffected. The result is a decrease in intensity of the feature at 8977.8 eV, which is more consistent with the experimental data. Crystallographic analysis of the *apo*- and *holo*-Ag(I) and *holo*-Cu(I) CusF binding sites shows flexibility in the orientation of the ligand residues and backbone, particularly for the methionines, which are the most solvent exposed residues in the metal binding site.[17,19] Therefore, a contraction of the S−Cu−S angle is certainly one possible origin of the discrepancy between the experimental and calculated spectra for CusF. Modulation of spectral intensities by varying metal−ligand bond distance and geometry were also investigated but were

DOI: 10.1021/acs.inorgchem.5b02842
Inorg. Chem. 2016, 55, 3431−3439

found not to correlate with the overall experimental spectral line shape (section S7 of the Supporting Information).

Variation of p−d mixing via coordination geometry was also investigated in the Cu_H site (Figure 7). In particular, a comparison of T-shaped and trigonal-planar geometries for the His_3 site was carried out. Crystallographic analysis indicates a distorted T-shaped geometry for the Cu_H site.[3,4] At the T-shaped coordination limit, the imidazole ligands interact predominantly with the $d_{x^2-y^2}$ orbital, increasing the amount of p mixing and increasing the energy of the $d_{x^2-y^2}$ orbital. At the same time, ligand interaction with the d_{xy} orbital is minimized. The overall result is a drop in intensity and a shift to higher energy for the transition at 8977.2 eV, which is in contrast to what one observes in the experimental data. A theoretical model more consistent with experimental data is that of a trigonal-planar geometry, where both calculated features of the Cu_H site match experimental spectra. Therefore, in solution, the Cu_H site may be better described as having a more trigonal planar coordination geometry rather than a T shape. This is also more consistent with the preferred Cu(I) geometry.[19]

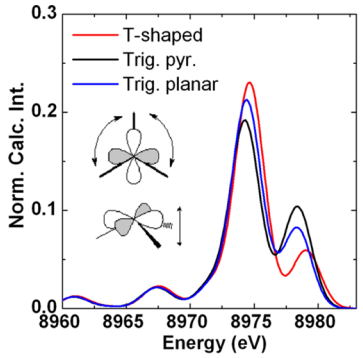

Model	$d_{x^2-y^2}$		d_{xy}	
	%d	%p	%d	%p
T-shaped	66.0	5.9	88.3	0
Trig. Pyramidal	76.4	4.3	75.4	4.2
Trig. Planar	75.9	3.2	78.3	3.6

Figure 7. (top) In silico study of the effect on the Cu_H VtC XES spectra of T-shaped, trigonal planar, and trigonal-pyramidal geometries and (inset) relative orientation of the $d_{x^2-y^2}$ orbital with respect to the ligands. (bottom) Percent Cu d and p character mixed in the d_{xy} and $d_{x^2-y^2}$ orbitals. Calculated spectra are shifted by 232 eV.

The above discussion highlights the possibility of using VtC XES, for electron-rich metal centers such as d^{10} systems, to gain insights into their coordination environment, in terms of both ligand speciation and site symmetry. This can complement sister techniques such as X-ray absorption, where it is often difficult to extract coordination geometry information for metal centers with filled d shells. This is due to the general lack of pre-edge features (1s → 3d) and rising edge features (1s → 4p) that depend on not only geometry but also covalency arguments.[47,54,55]

PHM-CO VtC XES Spectra. With an understanding of the factors affecting the spectral line shape, the applicability of VtC XES for exploring the PHM mechanisms was tested using CO-bound WT PHM (PHM-CO). Figure 8 shows the experimental spectra of PHM-CO superimposed with those of PHM. The spectrum of PHM was generated by averaging the spectra of the Cu_M site and Cu_H site. Two distinct differences are observed in the experimental spectra. PHM-CO has a more intense feature at 8978.3 eV attributed to transitions from the Cu d-manifold and a shoulder at 8969.5 eV, presumably due to the bound CO moiety. Calculated spectra of PHM and PHM-CO generally agree well with the experimental data (Figure 8-right).

To highlight the changes upon CO binding, both the experimental and calculated difference spectra of PHM-CO and PHM are overlaid in Figure 9. The Cu_M site of PHM-CO is a distorted tetrahedron. Crystallographic data highlight an elongation of the Cu−S bond for CO-bound Cu_M. Presumably this helps maintain the site closer to the trigonal-planar geometry favored by Cu(I), and similar behavior has previously been reported in proteins such as plastocyanin.[19,56] Nevertheless, a distorted-tetrahedral model is consistent with the experimental data. The increase in intensity in the Cu d region (**5**) of the VtC can be explained by the covalent interaction between the copper center and the CO ligand, resulting in more p−d mixing. Furthermore, two additional features at ∼8970 eV (**7**) and ∼8972.5 eV (**6**) are present and are consistent with previously reported VtC spectra of Fe-CO complexes (Figure 9). Complexes such as $[Fe(CO)_5]$ are reported to have two distinct features due to the CO moiety separated by ∼3 eV. The lower energy feature was assigned to metal interactions with the σ^*_{2s-2s} CO antibonding orbital, while the higher energy feature is attributed to the CO σ_{2p-2p} orbital.[39] The current result highlights that VtC XES is a

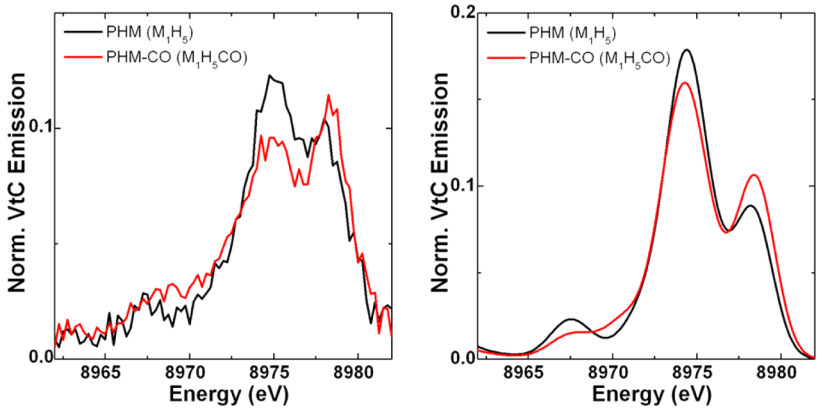

Figure 8. VtC XES spectra of PHM and PHM-CO: (left) experimental; (right) calculated. (M_1H_5) refers to the presence of both the Cu_M (M_1H_2) and Cu_H (H_3) sites. Calculated spectra are shifted by 232 eV.

DOI: 10.1021/acs.inorgchem.5b02842
Inorg. Chem. 2016, 55, 3431−3439

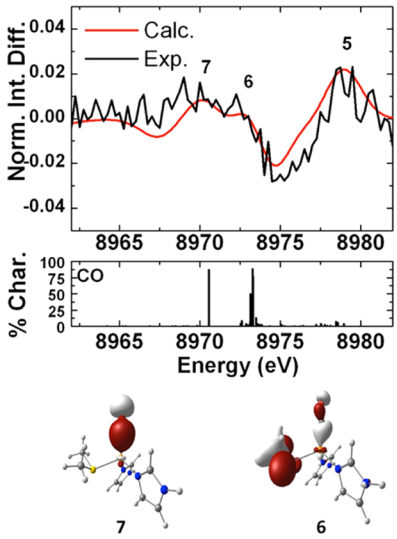

Figure 9. (top) Overlay of the experimental and calculated VtC XES difference spectra of PHM-CO and PHM. The calculated spectra are shifted by 232 eV. The truncated model was used. (middle) Percent character breakdown for individual transitions. (bottom) Molecular orbitals corresponding to features of interest (isovalue 0.05).

suitable approach to detected small-molecule interactions in PHM despite the presence of two nonequivalent Cu(I) sites.

SUMMARY AND CONCLUSION

Herein a series of Cu(I) metal binding sites with a systematic variation in ligand speciation (His/Met) were investigated with VtC XES. In all cases, a high-energy feature at ~8977 eV, attributed to transitions arising from filled Cu 3d orbitals, was observed. Computational analysis of this region demonstrated that the intensities of the Cu 3d transition are modulated by ligand -mediated Cu p−d mixing, through a configuration interaction mechanism. Sulfur-based ligands were found to more readily mix with the d manifold, resulting in more intense transitions in this region when methionines were present in comparison to those when histidines were present. This is facilitated by the presence of two Cu−ligand interactions with methionines: one from the S 3p lone pair and one from the S−CH_3 σ bond. In addition, both Cu(I) 3d transition energies and intensities can be modulated by the geometry around the metal and by the metal−ligand binding mode. Variations in geometry and/or binding mode of the ligand affect the overlap between the ligand and the d orbitals, altering the p−d mixing and thus the observed transition intensities. Therefore, in the case of electron-rich metal centers such as those having filled d^{10} shells, the VtC region might serve as a probe of not only ligand speciation but also coordination geometry, in a fashion similar to XAS pre-edges. Therefore, VtC XES could be used in conjunction with complementary techniques such as X-ray absorption to offer a more complete picture of the environment around the metal center. Finally, it was observed that VtC XES is sensitive to small-molecule coordination in PHM, suggesting it would be an appropriate method for future mechanistic studies.

ASSOCIATED CONTENT

Supporting Information

The Supporting Information is available free of charge on the ACS Publications website at DOI: 10.1021/acs.inorgchem.5b02842.

Representative fits of the experimental XES spectra, *XYZ* coordinates of the geometry-optimized protein metal sites as well as *XYZ* coordinates of the truncated models used for transition−orbital correlation, the models used for the impact of coordination geometry (CusB and PHM Cu_H), and overlays of the calculated VtC XES spectra from truncated and full metal site models as well as additional models tested for CusF (PDF)

AUTHOR INFORMATION

Corresponding Authors

*S.D.: e-mail, serena.debeer@cec.mpg.de.

*N.J.B.: e-mail, blackbni@ohsu.edu; tel, 503-346-3428; fax, 503-346-3427.

Present Addresses

[#]Group de Química Bioinorgànica, Supramolecular i Catàlisi (QBIS-CAT), Institut de Química Computacional i Catàlisi (IQCC), Departament de Química, Universitat de Girona, Campus Montilivi, 17071 Girona, Spain.

[▽]Department of Chemistry, Reed College, 3203 SE Woodstock Blvd., Portland OR 97202, United States.

[○]Inorganic Chemistry and Catalysis Group, Debye Institute for Nanomaterials Science, Utrecht University, 3584 CG Utrecht, The Netherlands.

[◆]Center for High Pressure Science & Technology Advanced Research #6-408, 1690 Cailun Rd., Pudong, Shanghai 201203, People's Republic of China.

Author Contributions

[⊥]These authors contributed equally to this work and should therefore be acknowledged as joint first authors.

Notes

The authors declare no competing financial interest.

ACKNOWLEDGMENTS

We thank Dr. Chelsey Kline and Ms. Mary Mayfield for assistance with PHM protein preparation and characterization. This work was funded by a grant from the National Institute of Health R01 GM115214 to N.J.B. K.N.C. was supported by the National Science Foundation Graduate Research Fellowship DGE-0925180. S.D. acknowledges the Max Planck Society for support. Use of the Stanford Synchrotron Radiation Lightsource, SLAC National Accelerator Laboratory, is supported by the U.S. Department of Energy, Office of Science, Office of Basic Energy Sciences, under Contract No. DE-AC02-76SF00515. The SSRL Structural Molecular Biology Program is supported by the DOE Office of Biological and Environmental Research and by the National Institutes of Health, National Institute of General Medical Sciences (including P41GM103393).

REFERENCES

(1) Klinman, J. P. *J. Biol. Chem.* **2006**, *281*, 3013.

(2) Prigge, S. T.; Mains, R. E.; Eipper, B. A.; Amzel, L. M. *Cell. Mol. Life Sci.* **2000**, *57*, 1236.

(3) Prigge, S. T.; Kolhekar, A. S.; Eipper, B. A.; Mains, R. E.; Amzel, L. M. *Science* **1997**, *278*, 1300.

DOI: 10.1021/acs.inorgchem.5b02842
Inorg. Chem. 2016, 55, 3431−3439

(4) Amzel, L. M.; Prigge, S. T.; Kolhekar, A. S.; Eipper, B. A.; Mains, R. E. *Nat. Struct. Biol.* **1999**, *6*, 976.
(5) Prigge, S. T.; Eipper, B. A.; Mains, R. E.; Amzel, M. *Science* **2004**, *304*, 864.
(6) Bauman, A. T.; Broers, B. A.; Kline, C. D.; Blackburn, N. J. *Biochemistry* **2011**, *50*, 10819.
(7) Blackburn, N. J.; Rhames, F. C.; Ralle, M.; Jaron, S. *JBIC, J. Biol. Inorg. Chem.* **2000**, *5*, 341.
(8) Boswell, J. S.; Reedy, B. J.; Kulathila, R.; Merkler, D. J.; Blackburn, N. J. *Biochemistry* **1996**, *35*, 12241.
(9) Chauhan, S.; Kline, C. D.; Mayfield, M.; Blackburn, N. J. *Biochemistry* **2014**, *53*, 1069.
(10) Chen, P.; Bell, J.; Eipper, B. A.; Solomon, E. I. *Biochemistry* **2004**, *43*, 5735.
(11) Chufan, E. E.; Prigge, S. T.; Siebert, X.; Eipper, B. A.; Mains, R. E.; Amzel, L. M. *J. Am. Chem. Soc.* **2010**, *132*, 15565.
(12) Jaron, S.; Blackburn, N. J. *Biochemistry* **1999**, *38*, 15086.
(13) Rudzka, K.; Moreno, D. M.; Eipper, B.; Mains, R.; Estrin, D. A.; Amzel, L. M. *JBIC, J. Biol. Inorg. Chem.* **2013**, *18*, 223.
(14) Grass, G.; Nies, D. H.; Franke, S. *Microbiology* **2001**, *147*, 965.
(15) Franke, S.; Grass, G.; Rensing, C.; Nies, D. H. *J. Bacteriol.* **2003**, *185*, 3804.
(16) Kittleson, J. T.; Loftin, I. R.; Hausrath, A. C.; Engelhardt, K. P.; Rensing, C.; McEvoy, M. M. *Biochemistry* **2006**, *45*, 11096.
(17) Loftin, I. R.; Franke, S.; Blackburn, N. J.; McEvoy, M. M. *Protein Sci.* **2007**, *16*, 2287.
(18) Loftin, I. R.; Franke, S.; Roberts, S. A.; Weichsel, A.; Heroux, A.; Montfort, W. R.; Rensing, C.; McEvoy, M. M. *Biochemistry* **2005**, *44*, 10533.
(19) Xue, Y.; Davis, A. V.; Balakrishnan, G.; Stasser, J. P.; Staehlin, B. M.; Focia, P.; Spiro, T. G.; Penner-Hahn, J. E.; O'Halloran, T. V. *Nat. Chem. Biol.* **2008**, *4*, 107.
(20) Bagai, I.; Liu, W.; Rensing, C.; Blackburn, N. J.; McEvoy, M. M. *J. Biol. Chem.* **2007**, *282*, 35695.
(21) Bagai, I.; Rensing, C.; Blackburn, N. J.; McEvoy, M. M. *Biochemistry* **2008**, *47*, 11408.
(22) Mealman, T. D.; Zhou, M.; Affandi, T.; Chacon, K. N.; Aranguren, M. E.; Blackburn, N. J.; Wysocki, V. H.; McEvoy, M. M. *Biochemistry* **2012**, *51*, 6767.
(23) Ucisik, M. N.; Chakravorty, D. K.; Merz, K. M., Jr. *Biochemistry* **2013**, *52*, 6911.
(24) Long, F.; Su, C. C.; Zimmermann, M. T.; Boyken, S. E.; Rajashankar, K. R.; Jernigan, R. L.; Yu, E. W. *Nature* **2010**, *467*, 484.
(25) Su, C. C.; Long, F.; Lei, H. T.; Bolla, J. R.; Do, S. V.; Rajashankar, K. R.; Yu, E. W. *J. Mol. Biol.* **2012**, *422*, 429.
(26) Su, C. C.; Long, F.; Zimmermann, M. T.; Rajashankar, K. R.; Jernigan, R. L.; Yu, E. W. *Nature* **2011**, *470*, 558.
(27) Chacon, K. N.; Mealman, T. D.; McEvoy, M. M.; Blackburn, N. J. *Proc. Natl. Acad. Sci. U. S. A.* **2014**, *111*, 15373.
(28) Pollock, C. J.; DeBeer, S. *Acc. Chem. Res.* **2015**, *48*, 2967.
(29) Bergmann, U.; Glatzel, P. *Photosynth. Res.* **2009**, *102*, 255.
(30) Lassalle-Kaiser, B.; Boron, T. T.; Krewald, V.; Kern, J.; Beckwith, M. A.; Delgado-Jaime, M. U.; Schroeder, H.; Alonso-Mori, R.; Nordlund, D.; Weng, T.-C.; Sokaras, D.; Neese, F.; Bergmann, U.; Yachandra, V. K.; DeBeer, S.; Pecoraro, V. L.; Yano, J. *Inorg. Chem.* **2013**, *52*, 12915.
(31) Lancaster, K. M.; Roemelt, M.; Ettenhuber, P.; Hu, Y.; Ribbe, M. W.; Neese, F.; Bergmann, U.; DeBeer, S. *Science* **2011**, *334*, 974.
(32) Pushkar, Y.; Long, X.; Glatzel, P.; Brudvig, G. W.; Dismukes, G. C.; Collins, T. J.; Yachandra, V. K.; Yano, J.; Bergmann, U. *Angew. Chem., Int. Ed.* **2010**, *49*, 800.
(33) Smolentsev, G.; Soldatov, A. V.; Messinger, J.; Merz, K.; Weyhermüller, T.; Bergmann, U.; Pushkar, Y.; Yano, J.; Yachandra, V. K.; Glatzel, P. *J. Am. Chem. Soc.* **2009**, *131*, 13161.
(34) Mijovilovich, A.; Hamman, S.; Thomas, F.; de Groot, F. M. F.; Weckhuysen, B. M. *Phys. Chem. Chem. Phys.* **2011**, *13*, 5600.
(35) Bauman, A. T.; Ralle, M.; Blackburn, N. *Protein Expression Purif.* **2007**, *51*, 34.
(36) Kline, C. D.; Mayfield, M.; Blackburn, N. J. *Biochemistry* **2013**, *52*, 2586.
(37) Sokaras, D.; Weng, T. C.; Nordlund, D.; Alonso-Mori, R.; Velikov, P.; Wenger, D.; Garachtchenko, A.; George, M.; Borzenets, V.; Johnson, B.; Rabedeau, T.; Bergmann, U. *Rev. Sci. Instrum.* **2013**, *84*, 053102.
(38) Delgado-Jaime, M. U.; Mewis, C. P.; Kennepohl, P. *J. Synchrotron Radiat.* **2010**, *17*, 132.
(39) Delgado-Jaime, M. U.; Debeer, S.; Bauer, M. *Chem. - Eur. J.* **2013**, *19*, 15888.
(40) Neese, F. *Wiley Interdisciplinary Reviews: Computational Molecular Science* **2012**, *2*, 73.
(41) Becke, A. D. *Phys. Rev. A: At., Mol., Opt. Phys.* **1988**, *38*, 3098.
(42) Perdew, J. P. *Phys. Rev. B: Condens. Matter Mater. Phys.* **1986**, *33*, 8822.
(43) Schäfer, A.; Horn, H.; Ahlrichs, R. *J. Chem. Phys.* **1992**, *97*, 2571.
(44) Weigend, F.; Ahlrichs, R. *Phys. Chem. Chem. Phys.* **2005**, *7*, 3297.
(45) Li, L.; Li, C.; Zhang, Z.; Alexov, E. *J. Chem. Theory Comput.* **2013**, *9*, 2126.
(46) Lee, N.; Petrenko, T.; Bergmann, U.; Neese, F.; Debeer, S. *J. Am. Chem. Soc.* **2010**, *132*, 9715.
(47) Kau, L. S.; Spira-Solomon, D. J.; Penner-Hahn, J. E.; Hodgson, K. O.; Solomon, E. I. *J. Am. Chem. Soc.* **1987**, *109*, 6433.
(48) Pollock, C. J.; DeBeer, S. *J. Am. Chem. Soc.* **2011**, *133*, 5594.
(49) Pollock, C. J.; Delgado-Jaime, M. U.; Atanasov, M.; Neese, F.; DeBeer, S. *J. Am. Chem. Soc.* **2014**, *136*, 9453.
(50) Bergmann, U.; Horne, C. R.; Collins, T. J.; Workman, J. M.; Cramer, S. P. *Chem. Phys. Lett.* **1999**, *302*, 119.
(51) MacMillan, S. N.; Walroth, R. C.; Perry, D. M.; Morsing, T. J.; Lancaster, K. M. *Inorg. Chem.* **2015**, *54*, 205.
(52) DeBeer George, S.; Brant, P.; Solomon, E. I. *J. Am. Chem. Soc.* **2005**, *127*, 667.
(53) Rees, J. A.; Martin-Diaconescu, V.; Kovacs, A. J.; Debeer, S. *Inorg. Chem.* **2015**, *54*, 6410.
(54) Penner-Hahn, J. E. *Coord. Chem. Rev.* **2005**, *249*, 161.
(55) Tomson, N. C.; Williams, K. D.; Dai, X.; Sproules, S.; DeBeer, S.; Warren, T. H.; Wieghardt, K. *Chemical Science* **2015**, *6*, 2474.
(56) Monari, A.; Very, T.; Rivail, J.-L.; Assfeld, X. *Comput. Theor. Chem.* **2012**, *990*, 119.

DOI: 10.1021/acs.inorgchem.5b02842
Inorg. Chem. 2016, 55, 3431−3439